Since January 2020 Elsevier has created a COVID-19 resource centre with free information in English and Mandarin on the novel coronavirus COVID-19. The COVID-19 resource centre is hosted on Elsevier Connect, the company's public news and information website.

Computers in Biology and Medicine 150 (2022) 106165

Contents lists available at ScienceDirect

Computers in Biology and Medicine

journal homepage: www.elsevier.com/locate/compbiomed

Two-step machine learning to diagnose and predict involvement of lungs in COVID-19 and pneumonia using CT radiomics

Pegah Moradi Khaniabadi [a,**], Yassine Bouchareb [a,*], Humoud Al-Dhuhli [a], Isaac Shiri [b], Faiza Al-Kindi [c], Bita Moradi Khaniabadi [d], Habib Zaidi [b,e,f,g], Arman Rahmim [h,i]

[a] Department of Radiology and Molecular Imaging, College of Medicine and Health Sciences, Sultan Qaboos University, PO. Box 35, PC123, Al Khoud, Muscat, Oman
[b] Division of Nuclear Medicine and Molecular Imaging, Geneva University Hospital, CH-1211 Geneva 4, Switzerland
[c] Department of Radiology, Royal Hospital, Muscat, Oman
[d] Child Growth and Development Research Center, Research Institute for Primordial Prevention of Non-communicable Disease, Isfahan University of Medical Sciences, Isfahan, Iran
[e] Geneva University Neurocenter, Geneva University, Geneva, Switzerland
[f] Department of Nuclear Medicine and Molecular Imaging, University of Groningen, University Medical Center Groningen, Groningen, Netherlands
[g] Department of Nuclear Medicine, University of Southern Denmark, Odense, Denmark
[h] Departments of Radiology and Physics, University of British Columbia, Vancouver, BC, Canada
[i] Department of Integrative Oncology, BC Cancer Research Institute, Vancouver, BC, Canada

ARTICLE INFO

Keywords:
COVID-19
Machine learning
Pneumonia
Radiomics
CT images
Diagnosis
Prediction

ABSTRACT

Objective: To develop a two-step machine learning (ML) based model to diagnose and predict involvement of lungs in COVID-19 and non COVID-19 pneumonia patients using CT chest radiomic features.
Methods: Three hundred CT scans (3-classes: 100 COVID-19, 100 pneumonia, and 100 healthy subjects) were enrolled in this study. Diagnostic task included 3-class classification. Severity prediction score for COVID-19 and pneumonia was considered as mild (0-25%), moderate (26-50%), and severe (>50%). Whole lungs were segmented utilizing deep learning-based segmentation. Altogether, 107 features including shape, first-order histogram, second and high order texture features were extracted. Pearson correlation coefficient (PCC≥90%) followed by different features selection algorithms were employed. ML-based supervised algorithms (Naïve Bays, Support Vector Machine, Bagging, Random Forest, K-nearest neighbors, Decision Tree and Ensemble Meta voting) were utilized. The optimal model was selected based on precision, recall and area-under-curve (AUC) by randomizing the training/validation, followed by testing using the test set.
Results: Nine pertinent features (2 shape, 1 first-order, and 6 second-order) were obtained after features selection for both phases. In diagnostic task, the performance of 3-class classification using Random Forest was 0.909 ±0.026, 0.907±0.056, 0.902±0.044, 0.939±0.031, and 0.982±0.010 for precision, recall, F1-score, accuracy, and AUC, respectively. The severity prediction task using Random Forest achieved 0.868±0.123 precision, 0.865 ±0.121 recall, 0.853±0.139 F1-score, 0.934±0.024 accuracy, and 0.969±0.022 AUC.
Conclusion: The two-phase ML-based model accurately classified COVID-19 and pneumonia patients using CT radiomics, and adequately predicted severity of lungs involvement. This 2-steps model showed great potential in assessing COVID-19 CT images towards improved management of patients.

1. Introduction

The COVID-19 pandemic has infected nearly 500 million individuals across the globe, with over 6 million death cases reported in the world [1]. Meticulous COVID-19 screening allows for early and accurate diagnosis, minimizing the impact on healthcare systems while also saving lives and limiting the spread of the disease [2,3]. Specifically, chest X-ray and CT scans are the first accurate diagnostic tools for determining the types of COVID-19 [4].

Radiomics analysis has great potential for precision medicine as it

* Corresponding author.
** Corresponding author.
E-mail addresses: pegah32121065@gmail.com (P. Moradi Khaniabadi), y.bouchareb@squ.edu.om, byassine06@yahoo.co.uk (Y. Bouchareb).

https://doi.org/10.1016/j.compbiomed.2022.106165
Received 5 July 2022; Received in revised form 18 September 2022; Accepted 1 October 2022
Available online 5 October 2022

uses data mining to create a correlation between clinical and biological findings [5,6]. Explicit radiomics features such as shape, statistics and texture are derived from medical images, resulting in accurate and non-invasive COVID-19 biomarkers that potentially influence clinical decision making. CT radiomics framework uses sophisticated quantitative features in CT images ("radiomics features") to describe types of lesions and tissue patterns [3,7]. These characteristics are grouped into two categories: semantic and agnostic characteristics. Agnostic features

Table 1
Examples of ML-based models for diagnosis, severity prediction and prognosis are presented in Table 1.

Year/ Ref.	Methods	Results	Conclusion	Advantage (Task)	limitations
2022/ [10]	Chest CT images of 176 patients. 63 quantitative features of the whole lung and the volume of ground-glass opacity regions, calculated. A RF model was trained to assess the severity based on quantitative features.	RF model showed 87% of accuracy, and 91% of AUC.	The RF based model can achieve automatic severity assessment of COVID-19 infection.	Severity prediction	Low sample size of patients with mild and critical types of COVID-19.
2021/ [11]	115 COVID-19 and 435 non-COVID-19 pneumonia patients. Key radiomics features extracted from chest CT images to build a radiomics signature using LASSO regression. Clinical and clinico-radiomics models were constructed. The combined model was further validated in the viral pneumonia cohort, and compared with performance of two radiologists using CO-RADS.	Combined radiomics model (radiomics + clinical variables) outperformed; an AUC of 98%. The combined model also performed better in distinguishing COVID-19 from other viral pneumonia with an AUC of 93%.	Preliminary study demonstrated the use of chest CT-based combined radiomics clinical model and CO-RADS in diagnosing COVID-19 pneumonia.	Diagnostic	(1) Data collected from two centers. (2) Enrolling the non-COVID pneumonia patients with blood laboratory pathogen-confirmation and pneumonia improvement after treatment by follow-up CT scans caused limited bacterial infection cases (3) Children with mycoplasma infections were included.
2020/ [12]	46 patients with COVID-19 and 29 other types of pneumonias. 77 radiomic features were extracted from the lesions. Four key features were screened and used as the inputs of SVM to build the radiomic signature. Multiple cross-validation was utilized to choose the primary characteristics following SVM as classifier to validate the AI-based model.	The model yielded AUCs of 86% for training and 82% in test set.	The model based on radiomics features could well discrimi-nate COVID-19 pneumonia from other pneumonias	Diagnostic	The preliminary study was based on data from a single hospital.
2021/ [7]	152 CT images of COVID-19 patients. radiological data, clinical data, and CT radiomics features combined to develop a novel prognostic models for prediction (alive, death).	Based on a multi-variate analysis, model obtained 0.95 AUC, 0.89 accuracy, 0.88 sensitivity and 0.89 specificity.	The combination of radiomic features, clinical and radiological data could effectively predict survival in COVID-19 patients.	Severity prediction	(1) Small sample size. (2) Therapeutic strategies for patients were excluded. (3) Only one feature selection and classifier algorithms were tested.
2020/ [13]	99 CT image sets of COVID-19 patients. The severity of disease was classified into three levels: moderate, severe, and critical. To identify the severity of the illness, they constructed RF and regression model.	The RF model obtained AUCs of 93% in the classification of both moderate vs. (severe + critical) and severe vs. critical.	CT quantification and machine-learning models show great potentials for assisting decision-making in the management of COVID-19 patients by assessing disease severity and predicting clinical outcomes.	Prognostic	(1) Small number of cases. (2) Using single-center data.
2022/ [14]	1110 CT image of COVID-19 patients. Four class severity scoring of severe-, moderate-, mild-, and non-pneumonic were studied. Radiomics Feature extraction performed in whole lung images.	They reported AUC of 0.846 (CI 95%: 0.805–0.887) using bagging random forest as feature selector and multinomial logistic regression as classifiers	Radiomics features of whole lung CT images were able to classify patients to the different severity class of COVID-19	Severity scoring, large data set, multiclass scoring	Only one radiologist scored images Single center datasets
2021/ [15]	14,339 CT scans of COVID-19 patients. Whole lung segmentations were performed using a DL-based model to extract 107 intensity and texture radiomics features. Several feature selection algorithms and classifiers were employed. Evaluation of models were examined using different splitting and cross-validation strategies using non-harmonized and ComBat-harmonized datasets.	ANOVA feature selector + RF classifier obtained AUC 83%. In ComBat harmonized dataset, Relief feature selector + RF classifier resulted in the highest performance of AUC, reaching 83%	Lung CT radiomics features could be used as biomarkers for prognostic modeling in COVID-19.	Prognostic, Large dataset	(1) Overlapping pneumonia regions in some CT images due to motion artifacts deficiency. (2) CT scans of typical manifestation of COVID-19 were used. (3) Clinical or laboratory data was excluded for developing the model (4) A prognostic model was developed based on all lung radiomics features only not all imaging manifestations in other organs. (5) Model developed without considering therapeutic regimens (6) To develop prognostic model, just binary classification was studied.

(e.g., textural features) apply creative mathematical processes in a high-throughput fashion that may not be possible to be detected by the human eye. Moreover, semantic features, such as shape, size, location, etc, are used to define morphologic properties of lesions. Artificial intelligence (AI) based methods, including Machine Learning (ML), have been used in several COVID-19 research studies [8,9]. In fact, ML-based models using CT-based radiomics, increasingly utilized for diagnosis, severity prediction, and prognosis of COVID-19 are straightforward and time efficient (Table 1).

In a large cohort multicenter study by CT radiomics features extracted from Lung regions and machine learning from 26,307 patients, prognostic [14] model was developed. Elsewhere [15], COVID-19 severity scoring was performed using CT radiomics features and multinomial multiclass machine learning models. More than thousand COVID-19 patient's data from four different class of severity were enrolled.

The latest studies have focused on either employing explicit radiomics to diagnose and differentiate COVID-19 pneumonia from other viral pneumonias or using ML techniques to stratify disease severity. However, to our knowledge, no research has been published on the validity of CT radiomics towards ultimate decision-making in the management of COVID-19 and pneumonia patients simultaneously in terms of diagnosis and severity prediction of clinical outcomes.

We there aimed to develop and deploy a two-phase ML radiomics signature approach. The model was developed based on radiomics features extracted exclusively from the whole lungs of CT images for differential diagnosis of COVID-19 and pneumonia to adequately evaluate their severity. Early diagnosis of COVID-19 and pneumonia etiology, particularly in patients with a highly suspected, may help clinicians in implementing appropriate patient management plans and reducing triage time during hospital admissions. In addition, severity prediction of COVID-19 and pneumonia, may help radiologists in making rapid diagnosis, that is particularly important when the healthcare system is overloaded. In what follows, we elaborate on our methods, followed by results, discussion, and conclusion.

2. Materials and methods

2.1. Data collection and segmentation

Imaging data from 300 CT scans (100 COVID-19 cases, 100 Pneumonia cases, and 100 Healthy ones) were collected from the Sultan Qaboos University Hospital (SQUH) and Royal Hospital (ROYH), Muscat, Oman. The SQUH and ROYH medical research ethical committees both approved this retrospective study (MREC#1254-REF. NO. SQU-EC/121/20). COVID-19 cases met the following criteria: (a) RT-PCR positive, (b) non-contrast CT on chest CT. Aside the COVID-19 group, ground truth of pneumonia cases was reviewed based on the radiologists' reports on CT images. CT Chest scans were performed on the Siemens Somatom definition flash 128 slices. Tube voltage, rotation time, and pitch were 120 kVp, 0.6 s, and 1.55, respectively. The reconstructed series matrix size was 512 × 512 pixels with 1 mm slice thickness. The scans were performed at maximum inspiration.

For segmenting whole lungs, DICOM CT images were segmented utilizing automated deep learning (DL) based segmentation for lungs and COVID-19 pneumonia infectious lesions (COLI-Net) which we have previously developed and extensively evaluated [16]. In this study we only employed the whole lung segmentation. Fig. 1 illustrates CT images and segmentations of Healthy, COVID-19 and pneumonia cases. All segmentations were evaluated by human observer to be sure about its accuracy and in case of mis-segmentation, segmentation was manually edited.

2.2. Severity scoring

The standardized score CO-RADS was utilized to assess the severity of infection of the whole lungs, enabling to analyze COVID-19 cases based on CT image findings [17]. Thus, for severity prediction, two experienced radiologists scored in consensus pulmonary involvement of COVID-19 RT-PCR positive and Pneumonia scans by percentage of involvement within all 5 lobes.

Most of CT demonstrations were described using standard nomenclature described by the Fleischner Society glossary and referring to the terms in literature on viral pneumonia and COVID-19 including ground glass opacity, crazy-paving pattern, and consolidation [18–20]. Based on involvement of the area of each lobe (right upper, right middle, right lower, left upper, and left lower), a semi-quantitative scoring method was employed to quantify the pulmonary involvement of all these abnormalities. Subsequently, they scored the type of pulmonary opacities such as ground-glass, mixed ground-glass and consolidation, consolidation, crazy paving appearance, etc. Scores were recorded as (a) 0: 0% involvement; (b) score 1: <5% involvement; (c) score 2: 5%–25% involvement; (d) score 3: 26%–50% involvement; (e) score 4: 51%–75% involvement; and (f) score 5: >75% lobar involvement). Total lungs involvement (labeled as subjective severity score) was concluded by adding the scores from all lobes (minimum score 0; maximum score 25) [21,22]. For developing the prediction model, the total lung infection involvement was classified into mild (0 <total score ≤10), moderate (11≤ total score ≤15), and severe (16 ≤ total score ≤25) as illustrated in Fig. 2.

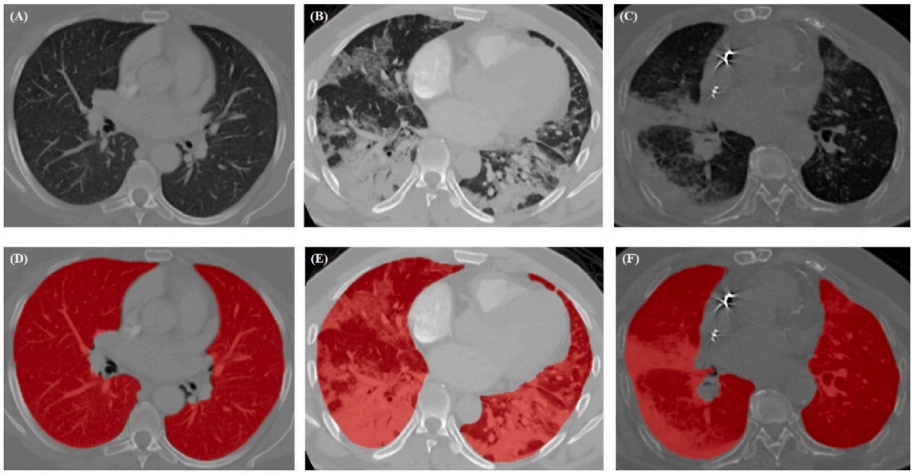

Fig. 1. Segmentation of Healthy (left); COVID-19 (middle); Pneumonia (right) utilizing our DL-based lungs segmentation method (COLI-Net).

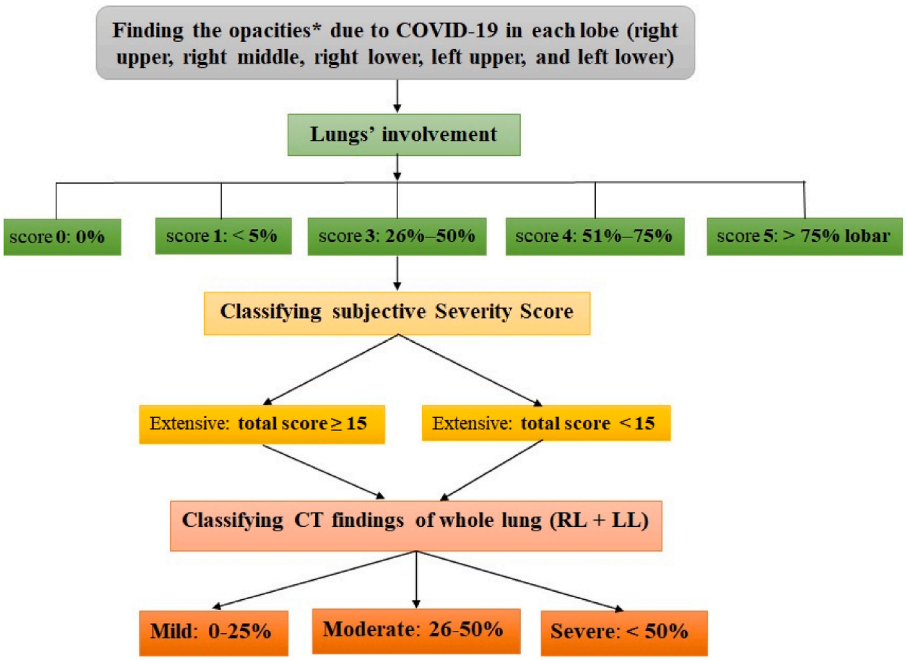

Fig. 2. A flowchart of severity scoring method. (*OPACITIES: Ground-glass, Mixed ground-glass and Consolidation, Consolidation, Reverse halo sign with ground-glass opacity surrounded by consolidation, Nodular, or Ground-glass with Crazy paving appearance. RL: Right Lung, LL: Left Lung).

2.3. Feature extraction and dimensionality reduction

The 107 features namely shape, first-order histogram, second and high order texture features, were generated using the Pyradiomics library [23]. All images were resized to isotropic voxel size $2 \times 2 \times 2\ mm^3$ and image intensity discretized by 64-Gy level binning, followed by feature extraction.

These features were divided into three categories: (i) intensity, (ii) shape, and (iii) texture. Lung intensity-based features, defined using first order statistics of the intensity histogram, quantified the tissue density of the right and left lungs on chest CT images. Shape features describe the 3D geometric properties of the lungs, whereas textural features quantified the infected region heterogeneity. Textural features were computed by analyzing the spatial distribution of voxel intensities in thirteen directions. Explicit features were computed from gray level co-occurrence (GLCM), run length matrices (GLRLM), Gray Level Dependence Matrix (GLDM), Gray Level Size Zone Matrix (GLSZM), and Neighborhood Gray-Tone Difference Matrix (NGTDM). It worth noting that the Pyradiomics image analysis software (PIAS) is part of the Image Biomarker Standardization Initiative (IBSI) [24].

To minimize overfitting and build a robust radiomics signature, dimensionally reduction (correlation-based feature selection method) reduced the number of features from 107 to 37. Further reduction to 9 features was achieved using the algorithm-based feature. The 9 most pertinent features include: shape features (2), first-order features (1), and second-order features (6), respectively. Spearman correlation, narrowed down the number of features to 37 features by removing redundant features [25]. To distinguish between informative features from redundant/noisy and irrelevant features 5 different supervised features selection algorithms using WEKA (version 3.8.2) were employed [26]. Then the results were compared utilizing voting method. In this step, 28 more features were eliminated. Hence, a set of 9 non-redundant and relevant features. Unlike other studies [27,28], the most pertinent features were finally selected using voting method by evaluating the

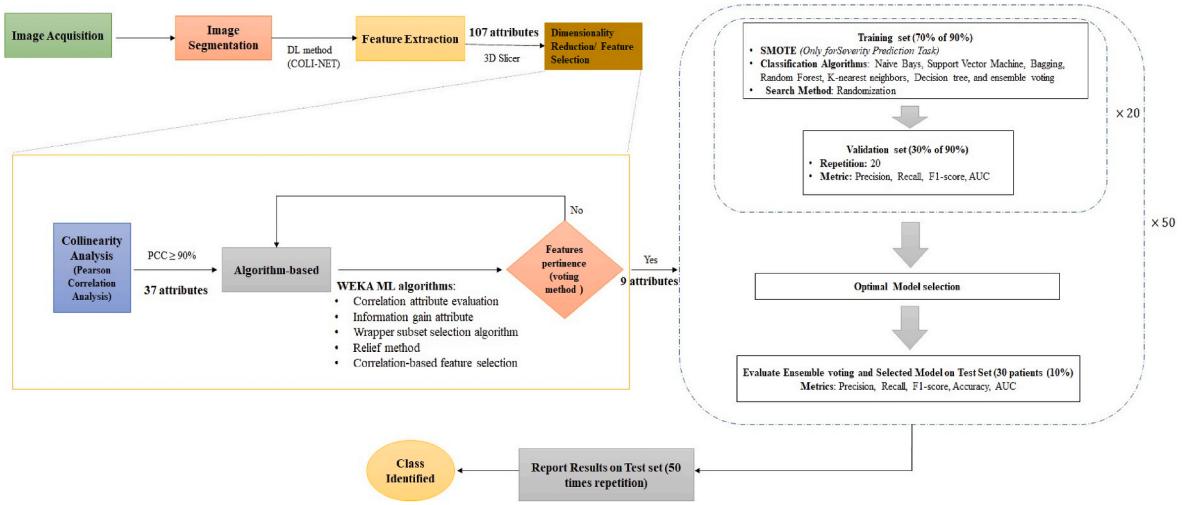

Fig. 3. An AI workflow in this study. Segmentation was performed using DL method while other steps were based on ML methods.

performances of algorithms. We have chosen features that were frequent among more than 4 algorithms in this performance assessment stage.

2.4. Model derivation and validation

2.4.1. Diagnostic phase

Datasets were randomly divided into 90% training sets and 10% test sets. The training set was used to select the best models (consistent with best practice guidelines) [29], and the test sets were used to report on the performance of the selected classifiers. The training sets was again split into 70% training and 30% validation sets; where the training set in this step of AI pipeline was used for learning and the validation set was used for giving an estimate of the model performance. Test sets were untouched during validation.

We considered several ML-based supervised algorithms namely Naïve Bays, Support Vector Machine, Bagging, Random Forest, K-nearest Neighbors, Decision Tree and Ensemble Meta Voting, as utilized through the WEKA toolkit. To select the optimal model based on precision, recall and AUC, we randomized training/validation sets 20 times. Splitting into training and validation set was performed 20 times to reduce variability in estimation of the model performance. The optimal model and Ensemble Meta Voting were then tested using the test set. We computed precision, recall, F1-score, accuracy, and AUC. To ensure the repeatability of the results, assessment using the test set, the entire operation was repeated 50 times.

The framework in Fig. 3 was first developed from scratch, step by step for the diagnosis task (classification as: COVID-19, Pneumonia or Healthy) and then using the same selected features (same 8 features mentioned above) we considered the 3 classes (mild, moderate, and severe) for the prediction step.

2.4.2. Prediction of severity phase

For severity prediction, two experienced radiologists scored involvement of lungs in COVID-19 and Pneumonia scans based on percentage of involvement in all 5 lobes. In severity prediction phase, previous datasets were classified into mild (0–25%), moderate (26–50%), and severe (>50%). In this second prediction phase the 300 datasets were randomly divided into 90% training set and 10% test sets. The training set was again split into 70% training and 30% validation sets, and test sets were untouched during validation. Prior to training, the synthetic minority oversampling technique (SMOTE) was used to balance the three classes (mild, moderate, severe). Note that for the diagnosis phase, the entire dataset was classified into 3 equal classes (healthy, COVID-19 and pneumonia), and therefore, SMOTE algorithm was only applied for the predication phase. Training and validation were performed as described in the diagnostic phase. Briefly, by using preselected radiomics, we considered several ML-based algorithms (as outlined in previous section). To select the optimal model based on precision, recall and AUC, we randomized training/validation sets 20 times. Splitting into training and validation set was performed 20 times to reduce variability in estimation of the model performance. The optimal model and ensemble meta voting tested using the test set. The model performance parameters (precision, recall, F1-score, accuracy, and AUC) were reposted. To ensure the repeatability of the results, assessment using the test set, the entire operation was repeated 50 times.

Overall, on chest CT scans, we extracted radiomic features associated

Fig. 4. Correlation matrix between the extracted features.

Table 2
Performance of several classifiers (mean(SD)) for the selection of the optimal model.

Classifier	Class	Precision	Recall	AUC
Random Forest	Healthy	0.907 (0.052)	0.977 (0.026)	0.990 (0.008)
	COVID-19	0.942 (0.049)	0.926 (0.060)	0.984 (0.017)
	Pneumonia	0.919 (0.054)	0.863 (0.072)	0.963 (0.022)
	Macro-Ave	**0.922 (0.017)**	**0.922 (0.057)**	**0.979 (0.014)**
Meta voting	Healthy	0.891 (0.063)	0.992 (0.019)	0.966 (0.017)
	COVID-19	0.927 (0.049)	0.935 (0.054)	0.944 (0.041)
	Pneumonia	0.932 (0.056)	0.826 (0.076)	0.890 (0.038)
	Macro-Ave	0.916 (0.022)	0.917 (0.084)	0.933 (0.039)
Naïve Bays	Healthy	0.824 (0.047)	0.998 (0.005)	0.968 (0.018)
	COVID-19	0.760 (0.076)	0.902 (0.065)	0.969 (0.021)
	Pneumonia	0.866 (0.079)	0.562 (0.098)	0.874 (0.042)
	Macro-Ave	0.816 (0.053)	0.82(0.229)	0.937 (0.054)
Support Vector Machine	Healthy	0.815 (0.050)	0.964 (0.051)	0.945 (0.027)
	COVID-19	0.821 (0.071)	0.855 (0.037)	0.907 (0.043)
	Pneumonia	0.823 (0.075)	0.656 (0.080)	0.774 (0.047)
	Macro-Ave	0.819 (0.004)	0.825 (0.156)	0.875 (0.089)
K-nearest-neighbor	Healthy	0.931 (0.047)	0.927 (0.058)	0.943 (0.027)
	COVID-19	0.896 (0.058)	0.923 (0.064)	0.932 (0.040)
	Pneumonia	0.871 (0.074)	0.841(0.08)	0.877 (0.048)
	Macro-Ave	0.899 (0.030)	0.897 (0.048)	0.917 (0.035)
Bagging	Healthy	0.831 (0.066)	0.962 (0.046)	0.979 (0.016)
	COVID-19	0.880 (0.083)	0.864 (0.073)	0.969 (0.023)
	Pneumonia	0.838 (0.087)	0.734 (0.103)	0.922 (0.035)
	Macro-Ave	0.849 (0.026)	0.853 (0.114)	0.956 (0.030)
Decision Tree	Healthy	0.874 (0.061)	0.909 (0.076)	0.942 (0.035)
	COVID-19	0.889 (0.065)	0.897 (0.097)	0.924 (0.044)
	Pneumonia	0.840 (0.095)	0.789 (0.091)	0.867 (0.056)
	Macro-Ave	0.867 (0.025)	0.865 (0.066)	0.911 (0.039)

with healthy, COVID-19, and pneumonia, which provides a noninvasive ML-based method to identify radiomic patterns of COVID-19 and pneumonia, differentiate COVID-19 from pneumonia and healthy (namely; "diagnostic phase" or phase 1), and predict COVID-19 and pneumonia severity (namely; "prediction of severity phase" or phase 2).

3. Results

To select non-redundant and relevant features, we carried out Spearman correlation coefficient (PCC $\geq$90%) and 5 different feature selection algorithms. Fig. 4 shows a set of 9 features (shape flatness; shape least length; first order kurtosis; GLCM cluster prominence; GLCM cluster shade; GLCM ImC1; GLDM small dependence high gray level emphasis; GLRLM run length nonuniformity; and GLSZM small area emphasis) were employed in constructing the two-phase ML-based model.

Table 2 and Fig. 5 summarize the results of optimum model selection with 20 times cross validation for each class (healthy, COVID-19, pneumonia). Random forest in comparison to the other classifiers achieved to best classification with precision = 0.922 (0.017), recall = 0.922 (0.057) and AUC = 0.0979 (0.014).

For the diagnostic task, the performance of the 3-class classification (healthy, COVID-19, pneumonia) using Random Forest and Meta Voting algorithm was assessed by computing precision, recall, F1-score, accuracy, and AUC. Table 3 shows the performance of the Random Forest and Meta Voting methods on test sets. The macro average scores for 3-class classification are provided to indicate the overall performance across the different classes of validation and test sets. From the validation utilizing Random Forest and Meta Voting, precision was 0.922 $\pm$ 0.017 and 0.916 $\pm$ 0.022, recall was 0.922 $\pm$ 0.057 and 0.917 $\pm$ 0.084 and AUC was 0.979 $\pm$ 0.014 and 0.933 $\pm$ 0.039, respectively. Moreover, based on the 3 $\times$ 3 confusion matrix, for RF and meta voting, the precision was 0.909 $\pm$ 0.026 and 0.894 $\pm$ 0.011, recall was 0.907 $\pm$ 0.056 and 0.897 $\pm$ 0.078, and AUC was 0.982 $\pm$ 0.010 and 0.922 $\pm$ 0.043, respectively in testing.

Similar to the diagnostic phase, the best model performance was achieved using the Random Forest algorithm. Furthermore, the performance of Random Forest and meta voting algorithms for severity prediction based on most pertinent radiomics was evaluated. Table 4 summarizes the performance of random forest and meta voting for severity prediction. It was also possible to classify CT scans with mild, moderate, and severe using random forest algorithm with the precision of 0.868 $\pm$ 0.123, recall of 0.865 $\pm$ 0.121, and AUC of 0.969 $\pm$ 0.022. Moreover, performance of severity prediction model using meta voting algorithm showed precision of 0.86 $\pm$ 0.123), recall of 0.849 $\pm$ 0.149, and AUC of 0.895 $\pm$ 0.072.

On the other hand, the performance validation metrics for the validation sets were precision of 0.917 $\pm$ 0.017, recall of 0.915 $\pm$ 0.044, and AUC of 0.98 $\pm$ 0.005. Moreover, performance of severity prediction model using meta voting algorithm showed precision of 0.913 $\pm$ 0.031, recall of 0.913 $\pm$ 0.035, and AUC (of 0.934 $\pm$ 0.015. The model accuracy and validation show how well model is generalizing.

4. Discussion

CT imaging scans have been widely used in COVID-19 studies. High quality 3D CT images have been utilized for COVID-19 identification and patient management. Since early days of the pandemic, numerous ML-based studies were focused on different tasks including diagnosing, prognostic, severity prediction utilizing binary or multiple classifications, using CT scans as illustrated in Table 5 [27,30–35].

In AI modeling for diagnosis, Huang et al. [37] analyzed the diagnostic value of CT-based signs combined with radiomics features to discriminate COVID-19 from other viral pneumonia. A total of 181 CT scans (89 COVID-19, and 92 non-COVID-19) were utilized. In the training and the testing cohort, the model achieved an AUC of 0.90 and 0.87, respectively.

In AI modelling for prediction, Pourhomayoun and Shakibi [38] used 7 different ML algorithms (logistic regression, support vector machine, decision tree, neural networks, random forest, and K-nearest neighbor) to predicted mortality risk of COVID-19 by using CT images. With an overall accuracy of 0.90, the Neural Network technique performed significantly better in predicting the death rate. Zhou et al. [39] employed a ML-based model to predict the progression of sickness severity. They used a genetic algorithm (GA) and support vector machine algorithm for feature selection and prediction, respectively.

In this study we utilized 9 explicit radiomics features using voting method to develop the 2 phase ML-based model for diagnosis and severity prediction of COVID-19 and pneumonia. Shape features illustrate properties of the size and shape of the images, which was found to

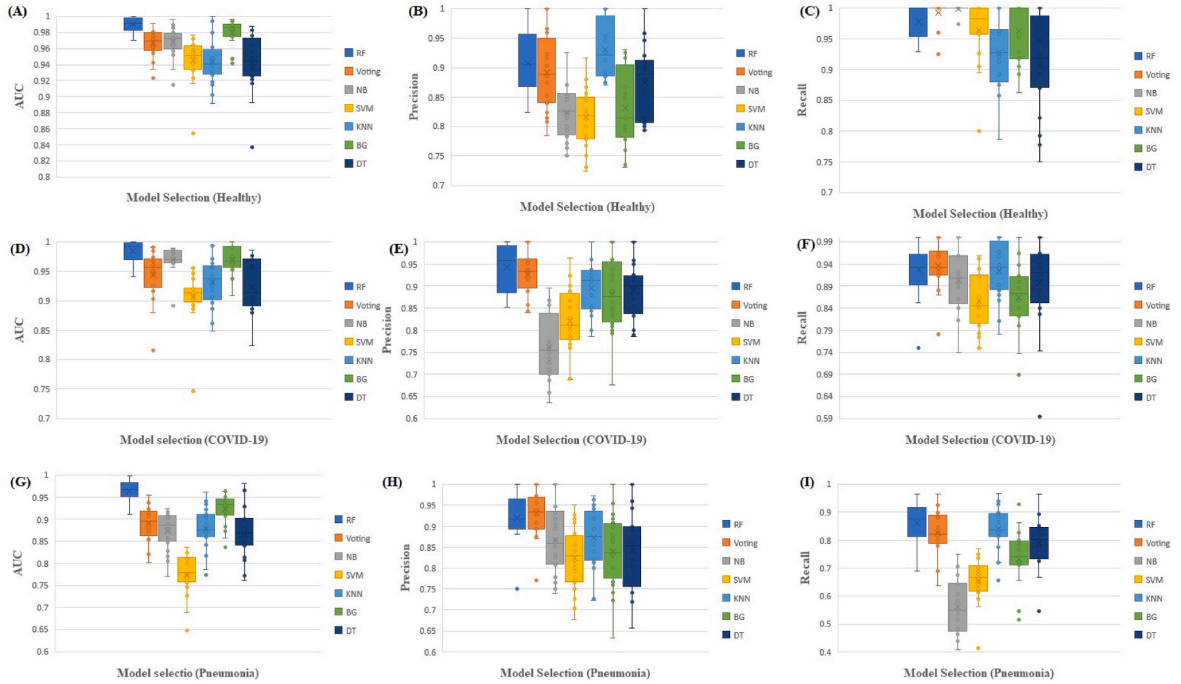

Fig. 5. Boxplots of the AUC, Precision, and recall for different classier algorithms and classifications; healthy (A,B,C), COVID-19 (D,E,F), pneumonia (G,H,I).

Table 3
Classification (healthy, COVID-19, pneumonia) performance (mean (SD)) indices by random forest and meta voting.

	Classifier	Class	Precision	Recall	F1-score	Accuracy	AUC
Test	**RF**	Healthy	0.934(0.090)	0.969(0.077)	0.951(0.065)	0.970(0.032)	0.993(0.011)
		COVID-19	0.913(0.010)	0.893(0.116)	0.894(0.079)	0.940(0.039)	0.984(0.020)
		Pneumonia	0.881(0.105)	0.859(0.111)	0.863(0.078)	0.908(0.046)	0.969(0.024)
		Macro-Ave	**0.909(0.026)**	**0.907(0.056)**	**0.902(0.044)**	**0.939(0.031)**	**0.982(0.010)**
	Meta voting	Healthy	0.908(0.104)	0.969(0.073)	0.934(0.077)	0.962(0.033)	0.964(0.044)
		COVID-19	0.888(0.097)	0.910(0.086)	0.893(0.05)	0.929(0.042)	0.927(0.043)
		Pneumonia	0.887(0.096)	0.813(0.119)	0.844(0.077)	0.894(0.049)	0.877(0.061)
		Macro-Ave	**0.894(0.011)**	**0.897(0.078)**	**0.89(0.045)**	**0.928(0.034)**	**0.922(0.043)**
Validation	**RF**	Healthy	0.907(0.052)	0.977(0.026)	0.939(0.026)	0.962(0.020)	0.990(0.008)
		COVID-19	0.942(0.049)	0.926(0.060)	0.94(0.037)	0.956(0.025)	0.984(0.017)
		Pneumonia	0.919(0.054)	0.863(0.072)	0.887(0.042)	0.919(0.024)	0.963(0.022)
		Macro-Ave	**0.922(0.017)**	**0.922(0.057)**	**0.922(0.030)**	**0.945(0.023)**	**0.979(0.014)**
	Meta voting	Healthy	0.891(0.063)	0.992(0.019)	0.938(0.031)	0.959(0.023)	0.966(0.017)
		COVID-19	0.927(0.049)	0.935(0.054)	0.930(0.037)	0.956(0.023)	0.944(0.041)
		Pneumonia	0.932(0.056)	0.826(0.076)	0.874(0.047)	0.914(0.024)	0.890(0.038)
		Macro-Ave	**0.916(0.022)**	**0.917(0.084)**	**0.914(0.034)**	**0.943(0.025)**	**0.933(0.039)**

Table 4
Classification (mild, moderate, severe) performance (mean (SD)) indices by random forest and meta voting.

	Classifier	Class	Precision	Recall	F1-score	Accuracy	AUC
Test	**RF**	Mild	0.958(0.058)	0.960(0.054)	0.957(0.039)	0.962(0.035)	0.987(0.018)
		Moderate	0.728(0.230)	0.729(0.233)	0.694(0.197)	0.915(0.050)	0.944(0.055)
		Severe	0.920(0.075)	0.908(0.081)	0.908(0.072)	0.927(0.049)	0.976(0.029)
		Macro-Ave	**0.868(0.123)**	**0.865(0.121)**	**0.853(0.139)**	**0.934(0.024)**	**0.969(0.022)**
	Meta voting	Mild	0.959(0.059)	0.965(0.053)	0.959(0.037)	0.965(0.032)	0.959(0.064)
		Moderate	0.722(0.242)	0.680(0.244)	0.663(0.202)	0.910(0.056)	0.816(0.122)
		Severe	0.899(0.092)	0.902(0.098)	0.894(0.075)	0.915(0.054)	0.911(0.062)
		Macro-Ave	**0.86(0.123)**	**0.849(0.149)**	**0.838(0.155)**	**0.93(0.030)**	**0.895(0.072)**
	RF	Mild	0.938(0.037)	0.965(0.031)	0.951(0.22)	0.961(0.017)	0.986(0.014)
Validation		Moderate	0.905(0.065)	0.902(0.050)	0.901(0.034)	0.946(0.019)	0.981(0.019)
		Severe	0.910(0.042)	0.880(0.057)	0.893(0.033)	0.928(0.021)	0.975(0.010)
		Macro-Ave	**0.917(0.017)**	**0.915(0.044)**	**0.915(0.031)**	**0.945(0.016)**	**0.98(0.005)**
	Meta voting	Mild	0.937(0.043)	0.946(0.032)	0.941(0.022)	0.955(0.016)	0.950(0.025)
		Moderate	0.878(0.070)	0.918(0.049)	0.850(0.199)	0.941(0.018)	0.935(0.023)
		Severe	0.924(0.048)	0.876(0.060)	0.897(0.038)	0.932(0.025)	0.919(0.031)
		Macro-Ave	**0.913(0.031)**	**0.913(0.035)**	**0.896(0.045)**	**0.942(0.011)**	**0.934(0.015)**

Table 5
ML-based models used in COVID-19.

Ref	Task	Model Training	Feature selection method	Modality/Subjects	Accuracy	Specificity	sensitivity	AUC
Xie et al. [21]	Diagnosis	LR	UA, LASSO	301 CT images, 33 COVID-19, 136 non-COVID-19, 48 malignant, 84 benign lesions of indeterminate nature	0.89	0.90	0.83	0.90
Chen et al. [26]	Diagnosis	MLR	LASSO	136 CT images, 70 COVID-19, 66 non-COVID-19	0.94 (95% CI 0.87–1.0)	0.94 (95% CI 0.87–1.0)	–	0.99 (95% CI 0.97–1)
Shi et al. [27]	Diagnosis	iSARF	–	2685 CT images, 1658 COVID-19, 1027 community acquired pneumonia	0.88	0.83	0.90	0.94
Rezaeijo et al. [28]	Diagnosis	RF	PC, RFE	194 CT images, 98 COVID-19, 96 suspected COVID-19	0.98	–	–	1.00
Shiri et al. [22]	Diagnosis	RF	ANOVA, KW, RFE	26,307 CT images, 15,146 COVID-19, 9657 non-COVID-19	0.96 (RF + Relief), 0.94 (RF + RFE), 0.94 (RF + ANOVA)	0.94 (RF + Relief), 0.93(RF + RFE),0.93(RF + ANOVA)	0.98 (RF + Relief), 0.96 (RF + RFE),0.96 (RF + ANOVA)	0.99 (RF + Relief), 0.98(RF + RFE), 0.98 (RF + ANOVA)
Yue et al. [29]	Prediction	LR, RF	–	31 CT images COVID-19	–	0.90 by LR, 1.0 by RF	1.0 by LR, 0.75 by RF	0.97 (95% CI, 0.83–1.0) by LR, 0.92 (95% CI, 0.67–1.0) by RF
Xu et al. [30]	Prediction	SVM	LASSO	284 CT images COVID-19, 75 early, 58 progressive, 75 severe, 76 absorption	–	–	–	0.90
Zhu et al. [31]	Prediction	RF	SFS, LASSO	408 CT images, COVID-19, 86 sever, 322 non-sever	0.86 ± 2.2	0.88 ± 1.45	0.77 ± 3.36	0.86 ± 2.27
Qiu et al. [32]	Prediction	SLR	LASSO	1160 CT images, COVID-19 infected pumonary	–	–	–	0.87
This study	Diagnosis and Prediction	RF, meta voting	SC, Voting	300 CT images, 100 COVID-19, 100 pneumonia, 100 Helathy	0.94 ± 0.031 and 0.92 ± 0.034 (diagnosis). 0.93 ± 0.024 and 0.93 ± 0.030 (prediction)	0.95 ± 0.020 and 0.95 ± 0.010 (diagnosis). 0.95 ± 0.011 and 0.95 ± 0.020 (prediction)	0.90 ± 0.056 and 0.90 ± 0.078 (diagnosis). 0.87 ± 0.121 and 0.85 ± 0.149 (prediction)	0.98 ± 0.010 and 0.92 ± 0.043 (diagnosis) 0.93 ± 0.024 and 0.93 ± 0.030 (prediction)

*LR: Logistic Regression, RF: Random Forest, MRL: Multi Linear Regression, SVM: Support Vector Machine, RFE: Recursive Feature Elimination, SLR: Stepwise Logistic Regression, KW: Kruskal-wallis, PC: Pearson Correlation, iSARF: infection Size Aware Random Forest method, LASSO: least absolute shrinkage and selection operator, UA: Univariate Analysis, SFS: Sample Feature Selection, SC: Spearman Correlation.

be effective in the classification/severity prediction of COVID-19 and pneumonia infections. Indication of shape feature dimensions was suggested to be investigated during each phase of COVID-19 [34,40,41].

First-order statistics represent the distribution of voxel intensities within the region of interest that significantly related to the pixel values on the CT scan through basic metrics. The first-order features mainly indicate the internal texture of lung regions [42]. Kurtosis is one of first-order features that is used to compute of the "peakedness" of the distribution of the values. Luís et al. [43] confirmed that COVID-19 induces consolidation and ground glass opacification, resulting in lower kurtosis values and flatter peak.

A gray level co-occurrence matrix (GLCM) provides the arrangement of voxel pairs to determine texture such as homogeneity (a reflection of the uniformity) of the distribution of voxels. Moreover, the gray run length matrix (GLRLM) provides the size of the uniform run per each gray level [44]. Recently, Hongmei et al. [45] illustrated that uniformity was less for COVID-19 than lesions in the non-COVID-19 class, with a greater range in irregular texture for the COVID-19 class. They indicated a more heterogeneous lung texture possibly on the grounds of diversity in airspace disease phenotypes such as crazy paving on visual inspection.

Moura et al. [43] observed more heterogeneity of GLRLM in the upper left region of COVID-19 class which may be due to consolidation that tended to diffuse. Pizzi et al. [40] predicted that the increasing homogeneity in COVID-19 might correlate with the degree of inflammatory infiltrate in the early stage of diffuse alveolar damage. In the severe phase, however, ground glass opacity develops in density and heterogeneity, forming a crazy paving pattern. The Gray Level Zone Length Matrix (GLZLM) gives parameters about the uniform zone size of each gray level in 3D or 2D region of interest. The gray-level nonuniformity of the COVID-19 group tended to be larger in compared to those of non-COVID-19 ones [44]. Moreover, GLSZM quantifies gray-level zones in an image as the number of connected voxels that share the same gray-level intensity.

For the first task (diagnosis), the validation of our 2 phase ML-based model utilizing RF and meta voting algorithms achieved AUCs of 0.979 ± 0.014 and 0.933 ± 0.039, respectively. For testing, RF and meta voting achieved AUCs of 0.982 ± 0.010 and 0.922 ± 0.043, respectively. Despite, for the second task (severity prediction) validation of our model achieved AUC of 0.969 ± 0.022 using RF algorithm and AUC of 0.895 ± 0.072 for meta voting. For testing, AUCs are 0.98 ± 0.005 and 0.934 ± 0.015 for RF and meta voting, respectively. The gap between the training and validation accuracy indicates the amount of overfitting [46]. In this study the percentage difference between accuracy of validation and testing for diagnosis task are 1.1% and 0.2% for RF and meta voting, respectively. Moreover, the gap between accuracy of validation and testing in severity prediction are 0.3% and 0.4% for RF and meta voting, respectively.

Despite addressing bias and limitations in establishing a generalizable model, some aspects should be considered in evaluating the results: (i) our proposed model is based on a medium sample size, however for

full generalizability, multi-centric/large datasets are required. As a result, using accurate data from the open source COVID-19 data repository could increase the model's accuracy; (ii) our model does not include clinical, demographic and laboratory data. However, previous studies showed significant correlation of CT radiomics with these findings [7,21,30,47]; (iii) we enrolled in-patient COVID-19 positive and pneumonia. Therefore, the moderate group was significantly lower than the mild and severe groups. To solve this issue, SMOTE algorithm was employed on training set only to obtain reproducible and repeatable performance; (iv) we did not include the impact of lesion biologic heterogeneity of lungs as well as the acquisition and reconstruction parameters on explicit CT radiomics features. However, COVID-19 diagnosis can result in considering infected pulmonary lesions in both lungs (right and left), reconstruction parameters have the potential to enhance the model performance [12,36,48]; (v) Despite the consensus that COVID-19 positive pulmonary involvement led to our chest CT severity scores. For determining the percentage of lung involvement in moderate and severe classes, other quantitative techniques, such as interrater reliability scores, may be helpful [49]. Future work should include different types of data (clinical and radiological) as prognostic indicators to develop a comprehensive model with a large sample size using multi-centre data to maximize the model performance.

5. Conclusion

CT radiomics features can be utilized towards derivation of biomarkers for COVID-19 and pneumonia diagnosis and severity prediction in a single 2-phase ML-based model. In terms of accuracy, the ML-based model demonstrated high performance in classifying COVID-19 and pneumonia (98%) cases using CT radiomics. In the second phase, an accuracy of 97% was achieved in classifying mild, moderate, and severe diseases. Our proposed, validated 2-phase model demonstrated great potential in assessing COVID-19 CT images towards rapid, reliable assessment and effective management of patients.

Disclosures

Nothing to disclose.

CRediT authorship contribution statement

Pegah Moradi Khaniabadi: Conceptualization, Methodology, Writing – original draft, Supervision, Revision, Approval the submitted version. **Yassine Bouchareb:** Conceptualization, Methodology, Writing – original draft, Supervision, Revision, Approval the submitted version. **Humoud Al-Dhuhli:** Revision, Provided clinical images, Approval the submitted version. **Isaac Shiri:** Revision, Scientific advice, Approval the submitted version. **Faiza Al-Kindi:** Revision, Provided clinical images, Approval the submitted version. **Bita Moradi Khaniabadi:** Methodology, Approval the submitted version. **Habib Zaidi:** Revision, Scientific advice, Approval the submitted version. **Arman Rahmim:** Methodology, Writing – review & editing. Guidance, Revision, Approval the submitted version.

Declaration of competing interest

None.

Acknowledgements

This work was supported by the Omani Research Council, Oman Grant, grant number RC/COVID-MED/RADI/20/01.

References

[1] Updates, COVID-19 coronavirus pandemic. https://www.worldometers.info/coronavirus september 2022.
[2] M. Dheyab, P. Khaniabadi, A. Aziz, et al., Focused role of nanoparticles against COVID-19: diagnosis and treatment, J Pd Pdt 34 (2021), 102287, https://doi.org/10.1016/j.pdpdt.2021.102287.
[3] Y. Boucharеb, P. Khaniabadi, F. Al Kindi, et al., Artificial intelligence-driven assessment of radiological images for COVID-19, J Comp Biomed 136 (2021), 104665, https://doi.org/10.1016/j.compbiomed.2021.104665.
[4] F. Wong, S. Lam, A. Fong, et al., Frequency and distribution of chest radiographic findings in patients positive for COVID-19, Radiology 296 (2) (2020) E72–E78, https://doi.org/10.1148/radiol.2020201160.
[5] M. Tomaszewski, J. Gillies, The biological meaning of radiomic features, Radiol. 298 (3) (2021) 505–516, https://doi.org/10.1148/radiol.2021202553.
[6] Y. Boucharеb, P. Khaniabadi, H. Al-Dhuhli, et al., Radiomics and artificial intelligence: how medical physicists can help their translation into radiology, molecular imaging and radiation therapy routine clinical practice? Phys. Med. 92 (2021) S38–S39, https://doi.org/10.1016/S1120-1797(22)00087-4.
[7] I. Shiri, M. Sorouri, P. Geramifar, et al., Machine learning-based prognostic modeling using clinical data and quantitative radiomic features from chest CT images in COVID-19 patients, Comp Biomed 132 (2021), 104304, https://doi.org/10.1016/j.compbiomed.2021.104304.
[8] A. Zargari, M. Heidari, S. Shariati, COVID-Classifier: an automated machine learning model to assist in the diagnosis of COVID-19 infection in chest x-ray images, Sci. Rep. 11 (1) (2021) 1–6, https://doi.org/10.1038/s41598-021-88807-2.
[9] L. Muhammad, A. Algehyne, S. Usman, et al., Supervised machine learning models for prediction of COVID-19 infection using epidemiology dataset, SN comput sci 2 (1) (2021) 1–13, https://doi.org/10.1007/s42979-020-00394-7.
[10] Z. Tang, W. Zhao, X. Xie, et al., Severity Assessment of Coronavirus Disease 2019 (COVID-19) Using Quantitative Features from Chest CT Images, 2020, https://doi.org/10.48550/arXiv.2003.11988 arXiv.
[11] H. Liu, H. Ren, Z. Wu, et al., CT radiomics facilitates more accurate diagnosis of COVID-19 pneumonia: compared with CO-RADS, J. Transl. Med. 19 (1) (2021) 1–12, https://doi.org/10.1186/s12967-020-02692-3.
[12] M. Fang, B. He, L. Li, D. Dong, X. Yang, C. Li, et al., CT radiomics can help screen the coronavirus disease 2019 (COVID-19): a preliminary study, Sci. China Inf. Sci. 63 (7) (2020) 1–8, https://doi.org/10.1007/s11432-020-2849-3.
[13] W. Cai, T. Liu, X. Xue, et al., CT quantification and machine-learning models for assessment of disease severity and prognosis of COVID-19 patients, Acad. Radiol. 27 (12) (2020) 1665–1678, https://doi.org/10.1016/j.acra.2020.09.004.
[14] I. Shiri, Y. Salimi, M. Pakbin, et al., COVID-19 prognostic modeling using CT radiomic features and machine learning algorithms: analysis of a multi-institutional dataset of 14,339 patients, Comput. Biol. Med. 145 (2022), 105467, https://doi.org/10.1016/j.compbiomed.2022.105467.
[15] I. Shiri, S. Mostafaei, A. Haddadi, et al., High-dimensional multinomial multiclass severity scoring of COVID-19 pneumonia using CT radiomics features and machine learning algorithms, Sci. Rep. 12 (1) (2022) 1–12, https://doi.org/10.1038/s41598-022-18994-z.
[16] I. Shiri, H. Arabi, Y. Salimi, et al., COLI-Net: deep learning-assisted fully automated COVID-19 lung and infection pneumonia lesion detection and segmentation from chest computed tomography images, IMA 32 (1) (2022) 12–25, https://doi.org/10.1002/ima.22672.
[17] M. Prokop, W. Van, T. van Rees, et al., CO-RADS: a categorical CT assessment scheme for patients suspected of having COVID-19—definition and evaluation, Radiol. 296 (2) (2020) E97–E104, https://doi.org/10.1148/radiol.2020201473.
[18] F. Pan, T. Ye, P. Sun, et al., Time course of lung changes on chest CT during recovery from 2019 novel coronavirus (COVID-19) pneumonia, Radiol. (2020), https://doi.org/10.1148/radiol.2020200370.
[19] M. Hansell, A. Bankier, H. MacMahon, et al., Fleischner Society: glossary of terms for thoracic imaging, Radiol. 246 (3) (2008) 697, https://doi.org/10.1148/radiol.2462070712.
[20] T. Franquet, Imaging of pulmonary viral pneumonia, Radiol. 260 (1) (2011) 18–39, https://doi.org/10.1148/radiol.11092149.
[21] F. Homayounieh, S. Ebrahimian, R. Babaei, et al., CT radiomics, radiologists, and clinical information in predicting outcome of patients with COVID-19 pneumonia, Radiol Cardio Imag 2 (4) (2020), e200322, https://doi.org/10.1148/ryct.2020200322.
[22] A. Bernheim, X. Mei, M. Huang, et al., Chest CT findings in coronavirus disease-19 (COVID-19): relationship to duration of infection, Radiol. (2020), https://doi.org/10.1148/radiol.2020200463.
[23] M. Tabatabaei, B. Tasorian, M. Goyal, et al., Feasibility of radiomics to differentiate coronavirus disease 2019 (COVID-19) from H1N1 influenza pneumonia on chest computed tomography: a proof of concept, ijms 46 (6) (2021) 420, https://doi.org/10.30476/ijms.2021.88036.1858.20.
[24] A. Zwanenburg, M. Vallières, A. Abdalah, et al., The image biomarker standardization initiative: standardized quantitative radiomics for high-throughput image-based phenotyping, Radiol. 295 (2) (2020) 328–338, https://doi.org/10.1148/radiol.2020191145.
[25] N. Papanikolaou, C. Matos, M. Koh, How to develop a meaningful radiomic signature for clinical use in oncologic patients, Cancer Imag. 20 (1) (2020) 1–10, https://doi.org/10.1186/s40644-020-00311-4.
[26] H. Seo, M. Badiei, V. Vasudevan, et al., Machine learning techniques for biomedical image segmentation: an overview of technical aspects and introduction to state-of-

art applications, Med phy 47 (5) (2020) e148–e167, https://doi.org/10.1002/mp.13649.
[27] C. Xie, M.-Y. Ng, J. Ding, et al., Discrimination of pulmonary ground-glass opacity changes in COVID-19 and non-COVID-19 patients using CT radiomics analysis, EJR (Eur. J. Radiol.) 7 (2020), 100271, https://doi.org/10.1016/j.ejro.2020.100271. Open.
[28] I. Shiri, Y. Salimi, A. Saberi, et al., Diagnosis of COVID-19 Using CT Image Radiomics Features: A Comprehensive Machine Learning Study Involving 26,307 Patients, 2021, https://doi.org/10.1101/2021.12.07.21267367 medRxiv.
[29] J. Bradshaw, R. Boellaard, J. Dutta, et al., Nuclear medicine and artificial intelligence: best practices for algorithm development, J. Nucl. Med. 63 (4) (2022) 500–510, https://doi.org/10.2967/jnumed.121.262567.
[30] X. Chen, Y. Tang, Y. Mo, et al., A diagnostic model for coronavirus disease 2019 (COVID-19) based on radiological semantic and clinical features: a multi-center study, Euro radiol 30 (9) (2020) 4893–4902, https://doi.org/10.1007/s00330-020-06829-2.
[31] F. Shi, L. Xia, F. Shan, et al., Large-scale screening to distinguish between COVID-19 and community-acquired pneumonia using infection size-aware classification, Phys. Med. Biol. 66 (6) (2021), 065031, https://doi.org/10.1088/1361-6560/abe838.
[32] M. Rezaeijo, M. Ghorvei, M. Alaei, et al., A Machine Learning Method Based on Lesion Segmentation for Quantitative Analysis of CT Radiomics to Detect Covid-19, IEEE, 2020, https://doi.org/10.1109/ICSPIS51611.2020.9349605.
[33] H. Yue, Q. Yu, C. Liu, et al., Machine learning-based CT radiomics method for predicting hospital stay in patients with pneumonia associated with SARS-CoV-2 infection: a multicenter study, atm 8 (14) (2020), https://doi.org/10.21037/atm-20-3026.
[34] Z. Xu, L. Zhao, G. Yang, et al., Severity assessment of COVID-19 using a CT-based radiomics model, Stem Cell. Int. (2021), https://doi.org/10.1155/2021/2263469.
[35] X. Zhu, B. Song, F. Shi, et al., Joint prediction and time estimation of COVID-19 developing severe symptoms using chest CT scan, Med. Image Anal. 67 (2021), 101824, https://doi.org/10.1016/j.media.2020.10182.
[36] J. Qiu, S. Peng, J. Yin, et al., A radiomics signature to quantitatively analyze COVID-19-infected pulmonary lesions, Interdiscip Sci 13 (1) (2021) 61–72, https://doi.org/10.1007/s12539-020-00410-7.
[37] Y. Huang, Z. Zhang, X. Li, et al., CT-based radiomics combined with signs: a valuable tool to help physician discriminate COVID-19 and other viral pneumonia, BMC Med. Imag. (2021), https://doi.org/10.1186/s12880-021-00564-w.
[38] M. Pourhomayoun, M. Shakibi, Predicting mortality risk in patients with COVID-19 using artificial intelligence to help medical decision-making, Smart Health (2021), https://doi.org/10.1016/j.smhl.2020.100178.
[39] K. Zhou, Y. Sun, L. Li, et al., Eleven routine clinical features predict COVID-19 severity uncovered by machine learning of longitudinal measurements, csbj 19 (2021) 3640–3649, https://doi.org/10.1016/j.csbj.2021.06.022.
[40] A. Delli, M. Chiarelli, P. Chiacchiaretta, et al., Radiomics-based machine learning differentiates “ground-glass” opacities due to COVID-19 from acute non-COVID-19 lung disease, Sci. Rep. 11 (1) (2021) 1–9, https://doi.org/10.1038/s41598-021-96755-0.
[41] F. Al-Areqi, Z. Konyar, Effectiveness evaluation of different feature extraction methods for classification covid-19 from computed tomography images: a high accuracy classification study, J bscp 2022 (2022), 103662, https://doi.org/10.1016/j.bspc.2022.103662.
[42] N. Chang, L. Cui, Y. Luo, et al., Development and multicenter validation of a CT-based radiomics signature for discriminating histological grades of pancreatic ductal adenocarcinoma, J qims 10 (3) (2020) 692, https://doi.org/10.21037/qims.2020.02.21.
[43] V. De Moura, C. Mattjie, M. Dartora, et al., Explainable machine learning for COVID-19 pneumonia classification with texture-based features extraction in chest radiography, J fdh (2022), https://doi.org/10.3389/fdgth.2021.662343.
[44] Y. Soleymani, R. Jahanshahi, M. Hefzi, et al., Evaluation of textural-based radiomics features for differentiation of COVID-19 pneumonia from non-COVID pneumonia, ejrnm (2021), https://doi.org/10.1186/s43055-021-00592-0.
[45] H. Wang, L. Wang, H. Lee, et al., Decoding COVID-19 pneumonia: comparison of deep learning and radiomics CT image signatures, ejnmmi 52 (1) (2021) 1–7, https://doi.org/10.1007/s00259-020-05075-4.
[46] D. Yang, C. Martinez, L. Visuña, et al., Detection and analysis of COVID-19 in medical images using deep learning techniques, Sci. Rep. 11 (1) (2021) 1–13, https://doi.org/10.1038/s41598-021-99015-3.
[47] C. Wungu, S. Khaerunnisa, E. Putri, et al., Meta-analysis of cardiac markers for predictive factors on severity and mortality of COVID-19, Int. J. Infect. Dis. 105 (2021) 551–559, https://doi.org/10.1016/j.ijid.2021.03.008.
[48] A. de Fátima Cobre, P. Stremel, R. Noleto, et al., Diagnosis and prediction of COVID-19 severity: can biochemical tests and machine learning be used as prognostic indicators? J Comp Biomed 134 (2021), 104531 https://doi.org/10.1016/j.compbiomed.2021.104531.
[49] R. Yang, X. Li, H. Liu, et al., Chest CT severity score: an imaging tool for assessing severe COVID-19, Radiol.: Cardio Imag 2 (2) (2020), https://doi.org/10.1148/ryct.2020200047.